

Neural Field Convolutions by Repeated Differentiation

NTUMBA ELIE NSAMPI, MPI Informatik, Germany
 ADARSH DJEACOMAR, MPI Informatik, Germany
 HANS-PETER SEIDEL, MPI Informatik, Germany
 TOBIAS RITSCHEL, University College London, United Kingdom
 THOMAS LEIMKÜHLER, MPI Informatik, Germany

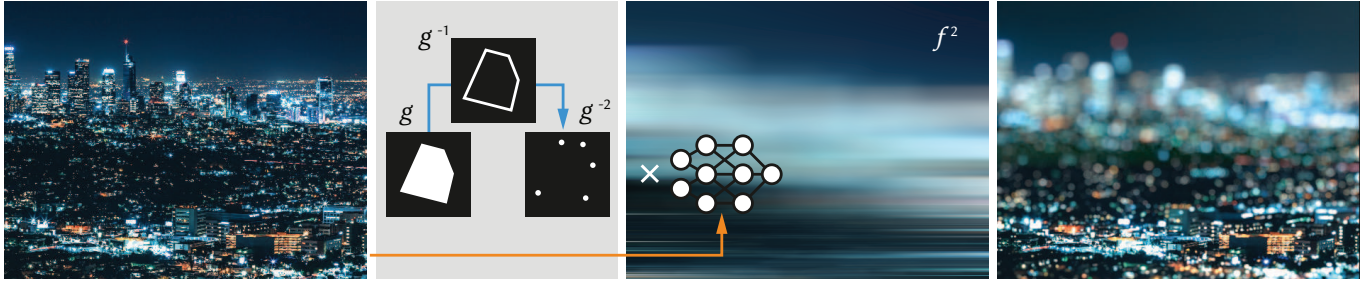


Fig. 1. We introduce an algorithm to perform efficient continuous convolution of a neural fields f by piecewise polynomial kernels g . The key idea is to perform convolution on the repeated derivative of the kernel (g^{-n}) and the repeated antiderivative of the signal (f^n).

Neural fields are evolving towards a general-purpose continuous representation for visual computing. Yet, despite their numerous appealing properties, they are hardly amenable to signal processing. As a remedy, we present a method to perform general continuous convolutions with general continuous signals such as neural fields. Observing that piecewise polynomial kernels reduce to a sparse set of Dirac deltas after repeated differentiation, we leverage convolution identities and train a repeated integral field to efficiently execute large-scale convolutions. We demonstrate our approach on a variety of data modalities and spatially-varying kernels.

1 INTRODUCTION

Neural fields have recently emerged as a powerful way of representing signals and have witnessed a widespread adoption in particular for visual data [Tewari et al. 2022; Xie et al. 2022]. Also referred to as implicit or coordinate-based neural representations, neural fields typically use a multi-layer perceptron (MLP) to encode a mapping from coordinates to values. This representation is universal and allows to capture a multitude of modalities, such as mapping from 2D location to color for images [Stanley 2007], from 3D location to the signed distance to a surface [Park et al. 2019], or from 5D light field coordinates to emitted radiance of an entire scene [Mildenhall et al. 2020], and many more.

The appealing properties of neural fields are three-fold: First, they represent signals in a continuous way, which is a good fit for the mostly continuous visual structure of our world. Second, they are compact, since they encode complex signals into a relatively small number of MLP weights, while adapting well to local signal complexities. Third, they are easy to optimize by construction. Taking all of these properties together, it comes at no surprise

that neural fields are rapidly evolving towards a general-purpose data representation [Dupont et al. 2022]. However, to be a true alternative to established specialized representations such as pixel arrays, meshes, point clouds, etc., neural fields are still lacking in a fundamental aspect: They are hardly amenable to *signal processing* [Xu et al. 2022; Yang et al. 2021]. As a remedy, in this work, we propose a general framework to apply a core signal processing technique to neural fields: convolutions.

The versatility and expressivity of neural representations has evolved significantly over the last couple of years, mostly due to advances in architectures and training methodologies [Hertz et al. 2021; Müller et al. 2022; Sitzmann et al. 2020; Tancik et al. 2020]. However, at their core, neural fields only support *point samples*. This is sufficient for point operations, such as the remapping of input coordinates, e.g., for the purpose of deformations [Kopanas et al. 2022; Park et al. 2021; Treitschke et al. 2021; Yuan et al. 2022], or the remapping of output values [Vicini et al. 2022]. In contrast, a convolution requires the *continuous integration* of values over coordinates weighted by a continuous kernel.

Aggregation in neural fields can be approximated using either discretization followed by cubature, or Monte Carlo sampling, resulting in excessive memory requirements and noise, respectively. Another solution is to consider a narrow parametric family of kernels and train the field using supervision on filtered versions of the signal [Barron et al. 2021]. Representation and learned convolution operation can be explicitly disentangled using higher-order derivatives [Xu et al. 2022], but this comes at the cost of only supporting small spatially-invariant kernels. AutoInt [Lindell et al. 2021] performs analytic integration using automatic differentiation, but only considers unweighted integrals. We advance the state of the art by presenting a method to *efficiently perform general, large-scale, spatially-varying convolutions natively* in neural fields.

Authors' addresses: Ntumba Elie Nsambi, MPI Informatik, Germany, nnsampi@mpi-inf.mpg.de; Adarsh Djeacomar, MPI Informatik, Germany, adjeacou@mpi-inf.mpg.de; Hans-Peter Seidel, MPI Informatik, Germany, hpseidel@mpi-sb.mpg.de; Tobias Ritschel, University College London, United Kingdom, t.ritschel@ucl.ac.uk; Thomas Leimkühler, MPI Informatik, Germany, thomas.leimkuehler@mpi-inf.mpg.de.

In our approach, we consider neural fields to be convolved with piecewise polynomial kernels, which reduce to a sparse set of Dirac deltas after repeated differentiation [Heckbert 1986]. Combining this insight with convolution identities on differentiation and integration, our approach requires only a small number of samples from a neural integral field to perform an exact continuous convolution, independent of kernel size. This integral field needs to be trained in a specific way, supervised via continuous higher-order finite differences, corresponding to a minimal kernel of a certain polynomial degree. Once trained, our neural fields are ready to be convolved with *any* piecewise polynomial kernel of that degree, positioning our method in the realm of zero-shot learning.

We showcase the generality and versatility of our approach using different modalities, such as images, videos, geometry, and character animations, all natively processed in a neural field representation. Further, we demonstrate (spatially-varying) convolutions with a large variety of kernels, such as smoothing and edge detection of different shapes and sizes.

In summary, our contributions are

- A principled and versatile framework for performing convolutions in neural fields.
- Two novel enabling ingredients: An efficient method to train a repeated integral field, and the optimization of continuous kernels that are sparse after repeated differentiation.
- The evaluation of our framework on a range of modalities and kernels.

2 RELATED WORK

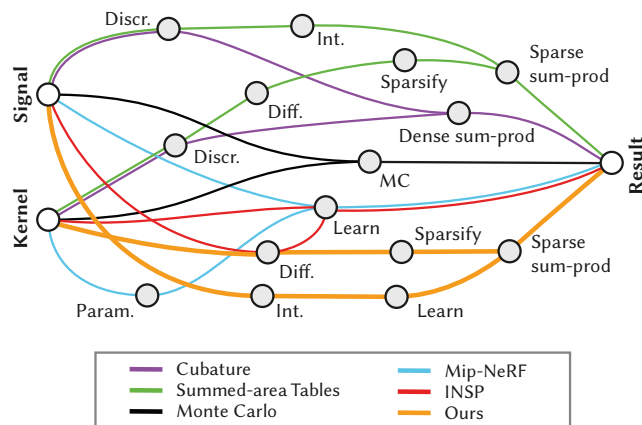


Fig. 2. The landscape of convolution methods: Every path pair of one color to connect signal and kernel (left) to the result (right) by combining basic operations (nodes) is a different convolution method.

The convolution of a signal, eventually in some higher dimension, with a kernel is a central operation in modern processing [Zhang 2022]. In this work, we consider a slightly more generalized form of convolution, where the kernel *varies spatially* across the signal.

Table 1. Comparison of different convolution methods. n is the size of the filter, m the size of the signal (samples or weights to represent it), and d the signal dimension.

	Time	Spat. vary	Noisy	Cont.
Classic	$O(m \times n^d)$	✓	×	×
Fourier	$O(m \times \log(m) \times d)$	×	×	×
Monte Carlo	$O(m \times n)$	✓	✓	✓
SAT	$O(m \times d)$	✓	×	×
Mip-NeRF	$O(m)$	✓	×	✓
INSP	$O(m)$	×	×	✓
Ours	$O(m)$	✓	×	✓

Discrete. For discrete signals and kernels (green and violet in Fig. 2), most convolutions are based on cubature across all dimensions. This, unfortunately, does not scale to larger kernels or higher dimensions, but allows spatially-varying kernels. A common acceleration is the *Fourier transform* [Brigham 1988], which also requires time and space to perform and store the transformed signal. Most of all, it requires the kernel to be spatially invariant. For a large class of filters, *pyramidal* schemes [Farbman et al. 2011; Williams 1983] can be a solution, but require additional memory. The key idea is that intermediate pyramid values store a partial aggregate of the signal. Techniques that store integrals without reducing the resolution are called *summed-area tables* (SAT) or *integral images* [Crow 1984; Viola and Jones 2001]. Notably, SATs allow efficient spatially-varying convolution by considering differentiated kernels [Heckbert 1986; Leimkühler et al. 2018; Simard et al. 1998]. This efficiency comes from the fact that the differentiated kernel is sparse (“Sparsify” along the green method in Fig. 2) and the SAT only needs to be evaluated at very few locations. Our approach will take this idea to the continuous neural domain.

Continuous. Convolution becomes more challenging, if the signal, the kernel, or both are continuous. *Monte Carlo* methods, that straightforwardly sample signal and kernel randomly and sum the result (black in Fig. 2) can handle this case. These scale very well to high dimensions, but at the expense of noise that only vanishes with many samples. Practical unstructured convolution [Hermosilla et al. 2018; Shocher et al. 2020; Vasconcelos et al. 2022; Wang et al. 2018] does away with cubature and evaluates the product of kernel and signal only at specific sparse positions such as the points in a point cloud. Our approach does not rely on random sampling but works directly on a continuous signal.

Neural. It has recently been proposed to replace discrete representations with continuous neural networks, so called *neural fields* [Tewari et al. 2022; Xie et al. 2022]. These have applications in geometry representation [Park et al. 2019], novel-view synthesis [Mildenhall et al. 2020; Sitzmann et al. 2019], dynamic scene reconstruction [Park et al. 2021; Treitsch et al. 2021; Yuan et al. 2022], etc. Replacing a discrete grid by complex continuous functions requires to develop the same operations available to grids [Dupont et al. 2022], including convolutions, so as we set out to do in this work. Early work has been conducted to explore the manifold of all natural neural fields [Du et al. 2021] and to build a generative

model of neural fields [Dupont et al. 2021]. Further, limited forms of geometry processing have been considered in this representation [Yang et al. 2021]. However, none of them is looking into efficient large-scale and/or spatially-varying convolutions.

A very specific form of convolution occurs as anti-aliasing or depth-of-field in image-based rendering. To account for these effects, neural fields can be learned that are conditioned on the parameters of the convolution kernel, such as its bandwidth [Barron et al. 2021, 2022; Isaac-Medina et al. 2022; Wang et al. 2022]. The network can then be evaluated to directly produce the filtered result, i.e., signal representation and convolution operation are intertwined. This Mip-NeRF-style convolution is in principle applicable to other filters, as long as they can be parametrized to become conditions to input into the network (blue in Fig. 2). Unfortunately, this limits the kernels that can be applied to a parametric family that needs to be known in advance, and burdens the cost of integration on the network. We use inductive knowledge of integration and differentiation to arrive at a more efficient formulation that generalizes across kernels.

The key to efficient convolutions is a combination of sparsity, differentiation and integration. Fortunately, tools to perform integration and differentiation on neural fields are available. AutoInt [Lindell et al. 2021] proposes to learn a neural network that, when automatically differentiated, fits a signal. By evaluating the original network without differentiation, the antiderivative can be evaluated conveniently. Unfortunately, this approach does not scale well to the higher-order antiderivatives needed for efficient convolutions, as the size of the derivative graphs grows quickly. In contrast, our approach leverages higher-order finite differences to train a repeated integral field, which scales with the number of integrations required.

Recently, Xu et al. [2022] (INSP) have proposed a method with the same aim as ours (red in Fig. 2). Given a trained neural field, they learn to combine higher-order derivatives of the field to approximate a convolution. Similar to a Taylor expansion, this approach requires high-order derivatives to reason about larger neighborhoods. Thus, unfortunately, this approach only allows for very small, spatially-invariant kernels.

Finally, aggregation in neural fields in the form of range queries has been studied by Sharp and Jacobson [2022]. Their approach allows to retrieve the field’s extrema within a query volume, which unfortunately does not provide enough information to perform accurate continuous convolutions.

3 BACKGROUND

We consider the convolution of arbitrary continuous signals $f \in \mathbb{R}^{d_{\text{in}}} \rightarrow \mathbb{R}^{d_{\text{out}}}$ with arbitrary continuous kernels $g \in \mathbb{R}^d \rightarrow \mathbb{R}$. Both inputs and outputs of f are low- to medium-dimensional. The signal can be any continuous function, including but not limited to a neural network. We assume the kernel has compact but potentially large support. The kernel does not necessarily extend across *all* input dimensions of f , i.e., $d \leq d_{\text{in}}$. To simplify our exposition, without loss of generality, we assume that the first d dimensions of f correspond to the filter dimensions of g . Further, we allow g to vary for different locations in the input space. An example of

this setup is a space-time signal f encoding an RGB ($d_{\text{out}} = 3$) video with two spatial and a temporal dimension ($d_{\text{in}} = 3$), to be convolved with a kernel g that applies a foveated blur to each time slice of the video ($d = 2$). In the following derivations, we assume a spatially-invariant kernel for ease of notation. Sec. 4.1.3 explains how our method can be easily extended to the spatially-varying case.

Formally, we seek to carry out the continuous convolutions

$$(f * g)(x) = \int_{\mathbb{R}^d} f(x - \tau)g(\tau)d\tau. \quad (1)$$

This integral operation does not have a closed-form solution for all but the most constrained sets of signals and/or kernels. In particular, it is unclear how this continuous operation can be applied to generic neural fields, which naturally only support point samples. The typical solution for these integrals is numerical approximation: For low-dimensional integration domains, quadrature rules are feasible, while the scalable gold standard in higher dimensions is Monte Carlo integration. The latter proceeds by sampling the integration domain and approximating the integral by a weighted sum of integrand evaluations:

$$(f * g)(x) = \mathbb{E}_{\tau} [f(x - \tau)g(\tau)] \approx \frac{1}{N} \sum_{\tau \sim p} \frac{f(x - \tau)g(\tau)}{p(\tau)}, \quad (2)$$

where \mathbb{E} is the expectation and τ are now random samples drawn from the probability density function p . Unfortunately, a high number N of samples is required for large kernels g and/or high-frequency signals f , rendering this approach inefficient.

In the following, we develop a method that performs continuous convolutions in the form of Eq. 1, while only requiring a very low number of network evaluations, independent of kernel size and signal complexity.

4 METHOD

We seek to efficiently convolve a continuous signal f with a continuous kernel g . We do so by approximating g with a piecewise polynomial function, which becomes sparse after repeated differentiation. Our approach requires the evaluation of the repeated integral of f at a sparse set of sample positions dictated by the differentiated kernel (Sec. 4.1). This leads to a substantial speed-up of the convolution operation, in particular for large g . We optimize for a sparse differential representation of g (Sec. 4.2), and obtain the repeated integral of f by supervising on a minimal kernel using higher-order finite differences (Sec. 4.3). Once trained, any sparsity-optimized convolution kernel can be applied to f efficiently, without requiring additional input parameters. Our method supports spatially-varying convolutions, as well as continuously transformed kernels, leveraging the continuous nature of the representation. Fig. 3 gives an overview of our approach.

4.1 Convolution by Repeated Differentiation

We rely on a sparsification of g to perform neural field convolutions with a runtime performance that is independent of both kernel size and field complexity. For this to work, we need two conceptual ingredients: First, the convolution operation in Eq. 1 reduces to a discrete sum if g consists of only Dirac deltas (Sec. 4.1.1). Second, the

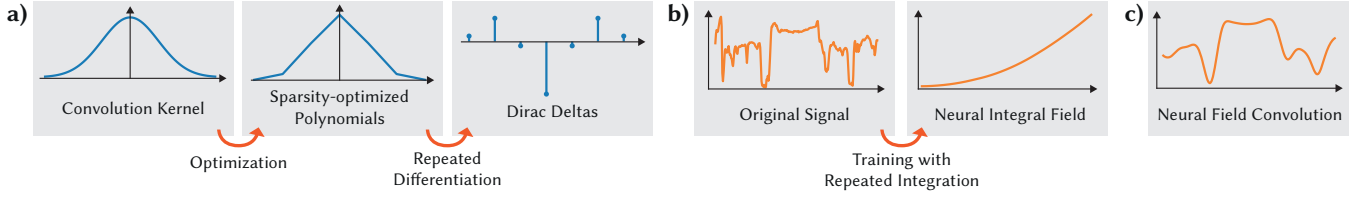


Fig. 3. Overview of our approach. *a)* Given an arbitrary convolution kernel, we optimize for its piecewise polynomial approximation, which under repeated differentiation yields a sparse set of Dirac deltas. *b)* Given an original signal, we train a neural field which captures the repeated integral of the signal. *c)* The continuous convolution of the original signal and the convolution kernel is obtained by a discrete convolution of the sparse Dirac deltas from *a)* and corresponding sparse samples of the neural integral field from *b)*.

right-hand side of Eq. 1 can be transformed using repeated differentiation and integration (Sec. 4.1.2). Putting both ingredients together leads to an efficient discrete formulation of the continuous convolution operation (Sec. 4.1.3) involving a repeated integral field and a sparse differential kernel consisting of Dirac deltas.

4.1.1 Dirac Kernels. As our first ingredient, consider a kernel g that is non-zero only at a small set of m locations in \mathbb{R}^d , i.e., g is a sum of Dirac deltas δ :

$$g(x) = \sum_{i=1}^m \delta(x - x^{(i)})w^{(i)}, \quad (3)$$

where $x^{(i)} \in \mathbb{R}^d$ denotes the location and $w^{(i)} \in \mathbb{R}$ the magnitude¹ of the i 'th impulse. Then, by the *sifting* property of Dirac deltas, Eq. 1 simplifies to

$$(f * g)(x) = \sum_{i=1}^m f(x - x^{(i)})w^{(i)}, \quad (4)$$

i.e., we have reduced the computation from a continuous integral to a discrete sum – an efficient operation if m is small.

4.1.2 Convolutions with Differentiation and Integration. Our second ingredient is the following identity:

$$f * g = \left(\int f dx_i \right) * \left(\frac{\partial}{\partial x_i} g \right),$$

i.e., in order to convolve f with g we might as well convolve the antiderivative of f with the corresponding derivative of g . We refer to Heckbert [1986] for a proof. Applying this principle repeatedly yields

$$f * g = \underbrace{\left(\int \dots \int f dx_1^n \dots dx_d^n \right)}_{f^n} * \underbrace{\left(\frac{\partial^{dn}}{\partial x_1^n \dots \partial x_d^n} g \right)}_{g^{-n}}. \quad (5)$$

Here, we sequentially differentiate g n times with respect to *each* of its dimensions. We denote this multidimensional repeated derivative as g^{-n} . For equality in Eq. 5 to hold, this pattern is mirrored for f , replacing differentiations with antiderivatives, where superscripts n denote repeated integrations along the individual dimensions. We denote the repeated multidimensional antiderivative of f as f^n .

¹Technically, $\delta(0) = \infty$. But since a Dirac delta integrates to one, in the context of continuous convolutions, we refer to $w^{(i)}$ as “magnitudes” nevertheless.

4.1.3 Efficient Neural Field Convolutions. The central idea of our approach is to combine both ingredients presented above for the case of piecewise polynomial kernels \hat{g} . Concretely, we observe that piecewise polynomial functions turn into a sparse set of Dirac deltas after repeated differentiation [Heckbert 1986] (Fig. 4), i.e., \hat{g}^{-n} reduces to the form of Eq. 3. This implies that Eq. 4 can be used to perform a convolution with this kernel. Combining Eq. 4 and Eq. 5, our final convolution operation reads

$$(f * \hat{g})(x) = \sum_{i=1}^m f^n(x - x^{(i)})w^{(i)}. \quad (6)$$

Notice that this formulation requires only m evaluations of the repeated integral of f at locations dictated by the Dirac deltas of the differentiated kernel to yield the same result as the equivalent continuous convolution in Eq. 1.

The number of integrations and differentiations n directly depends on the desired order of the kernel polynomials, as detailed in Sec. 4.2. A disk-shaped kernel simulating thin-lens depth of field in an image can be approximated well using a piecewise *constant* function (corresponds to $n = 1$), while a Gaussian might require a piecewise *quadratic* approximation (corresponds to $n = 3$) to yield high-quality results with a low number of Dirac deltas.

Notice that our approach allows to realize *spatially-varying* convolutions as well: The evaluation of Eq. 6 is independent for different evaluation locations x . Therefore, we can make the choice of the convolution kernel \hat{g} a function of x itself. In Sec. 4.2.2 we give details on how to obtain continuous parametric kernel families.

In summary, our method requires two components: *(i)* A piecewise polynomial kernel which results in a sparse set of Dirac deltas after repeated differentiation, and *(ii)* an efficient way to obtain and evaluate the repeated multidimensional integral of a continuous signal. These components are detailed in Sec. 4.2 and Sec. 4.3, respectively.

4.2 Sparse Differential Kernels

Our approach requires a kernel g which, after repeated differentiation, results in a sparse set of Dirac deltas with positions $x^{(i)}$ and magnitudes $w^{(i)}$:

$$g^{-n}(x) = \sum_{i=1}^m \delta(x - x^{(i)})w^{(i)}. \quad (7)$$

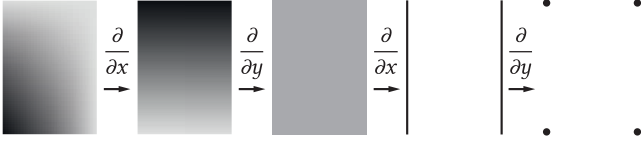


Fig. 4. Repeated differentiation of a bilinear patch ($d = n = 2$). After the first differentiation w.r.t. x , the patch only exhibits linear variation along the vertical dimension. A subsequent differentiation w.r.t. y makes the patch constant. A subsequent differentiation w.r.t. x results in two vertical lines, while the final differentiation w.r.t. y produces four Dirac deltas at the corners of the original patch.

This property is satisfied for piecewise polynomial kernels of degree $n - 1$, which reduce to Dirac deltas positioned at the junctions between the segments after n differentiations per dimension [Heckbert 1986] (Fig. 4). Thus, given a kernel g , we seek to find its optimal piecewise polynomial approximation \hat{g} adhering to a user-specified budget of m Dirac deltas (Fig. 5).

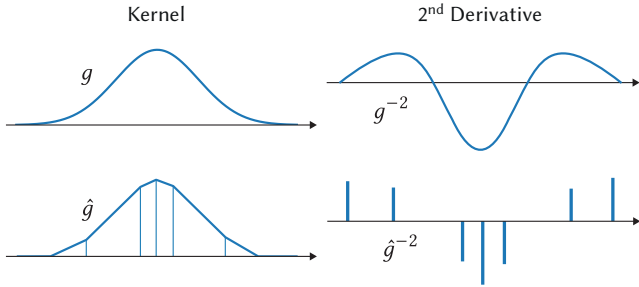


Fig. 5. Kernel representation in 1D for the case $n = 2$, i.e., a piecewise linear function. *Top row*: The original continuous kernel g has a continuous second derivative. *Bottom row*: We approximate g with a piecewise linear function \hat{g} , which reduces to a sparse set of Dirac deltas in its second derivative.

To parameterize \hat{g} , we utilize the linear structure of Eq. 7 and the linearity of differentiation: We consider the d -dimensional n -fold repeated antiderivative of the Dirac delta function

$$\delta^n(\mathbf{x}) = \begin{cases} \frac{\prod_{i=1}^d x_i^{n-1}}{(n-1)^d!} & \min_i x_i \geq 0 \\ 0 & \text{else} \end{cases}$$

which is referred to as the n 'th-order *ramp* (Fig. 6). We now write our polynomial kernel \hat{g} as a linear combination of shifted ramps:

$$\hat{g}(\mathbf{x}) = \sum_{i=1}^m \delta^n(\mathbf{x} - \mathbf{x}^{(i)}) w^{(i)}. \quad (8)$$

Please note that Eq. 7 is the n 'th derivative of Eq. 8 by construction. Thus, we have established a parameterization of a C^{n-2} -continuous piecewise polynomial kernel \hat{g} , from which we can directly read off Dirac delta positions and magnitudes.

We now optimize the following objective:

$$\min_{\mathbf{x}^{(i)}, w^{(i)}} \left[\mathbb{E}_{\mathbf{x} \in \mathbb{R}^d} [\|g(\mathbf{x}) - \hat{g}(\mathbf{x})\|_2^2] + \lambda \sum_{i=1}^m w^{(i)} \right]. \quad (9)$$

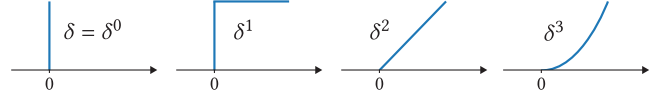


Fig. 6. 1D ramps of different orders (redrawn from Heckbert [1986]). Each ramp is the antiderivative of its predecessor.

The first term encourages the solution to be close to the reference kernel on the entire domain. The second term steers the optimization to prefer solutions where the Dirac magnitudes sum to zero, which effectively enforces the kernel to be compact.

4.2.1 Optimization. We initialize the ramp positions $\mathbf{x}^{(i)}$ on a regular grid and their magnitudes $w^{(i)}$ to zero. We use the Adam [Kingma and Ba 2014] optimizer with standard parameters and set $\lambda = 0.1$ in all our experiments. In each iteration, we uniformly sample the continuous kernel domain. We observe that when the provided ramp budget m is too high, the magnitudes of individual ramps will approach zero, further increasing sparsity. We capitalize on this fact by monitoring ramp magnitudes in regular intervals. If an absolute magnitude falls below a small threshold, we remove the ramp from the mixture and continue optimizing. Separable kernels can be obtained by optimizing the respective 1D filters and combining them with an outer product. The entire process takes less than a minute in our un-optimized implementation.

4.2.2 Kernel Transformations. Many applications of convolutions require kernels of different sizes and shapes, in particular in the case of spatially-varying convolutions. For example, foveated imagery or the simulation of depth-of-field require continuous and fine-grained control over the size of a blur kernel. Our approach supports on-the-fly kernel transformations without the need to sample and optimize entire parametric families of kernels by leveraging the continuous nature of the kernel and the signal.

Concretely, to continuously shift and (anisotropically) scale an optimized kernel \hat{g} using a matrix T , we simply apply T to the Dirac delta positions, i.e., $\mathbf{x}_T^{(i)} = T\mathbf{x}^{(i)}$. The updated Dirac delta magnitudes are given by $w_T^{(i)} = \frac{w^{(i)}}{\det(T)^n}$. Thus, we need to run the optimization for a kernel type only once in a canonical position and size, and obtain continuously transformed kernel instances at virtually no computational cost. Notice that, as a useful consequence, our approach enables continuous scale-space analysis [Lindeberg 2013; Witkin 1987].

4.3 Neural Repeated Integral Field

To compute Eq. 6, we need to evaluate f^n , the n -th antiderivative of f as the second ingredient. We choose to implement f^n as a neural field \hat{f}^n . Ideally, it would hold that $\hat{f}^n = f^n$. This might be difficult to achieve without knowing an analytic form of the antiderivative. We could try Monte Carlo-estimating the antiderivative from the signal, leading to a loss like

$$\mathbb{E}_{\mathbf{x} \in d_{\text{in}}} \left[\left\| \hat{f}^n(\mathbf{x}) - \mathbb{E}_{\tau \geq 0} [f(\mathbf{x} - \boldsymbol{\tau})] \right\| \right]. \quad (10)$$

The inner expectation would sum over the entire half-domain $\tau \geq 0$, leading to a high variance and a low-quality \hat{f}^n . An example of

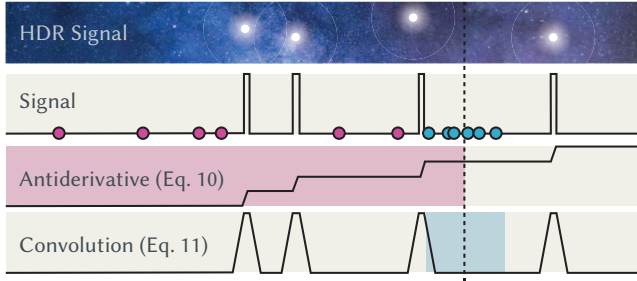


Fig. 7. Antiderivative loss estimation: The first row shows an HDR image with four stars. These are four box-peaks in the second row, showing a scanline of that image. To compute any value for the antiderivative in the third row, (dotted line) we need to sum all integrand (signal) values to the left, the entire red area. This will miss peaks. The fourth row shows an alternative loss, that supervises on a convolution with a minimal kernel. It only requires samples in the small, blue area, which will not miss a star.

this is shown in Fig. 7: Input is a HDR signal, an image of a night sky, with stars forming four peaks. To estimate the antiderivative loss at the dotted line, we have to sample the entire pink area with pink samples, that are unlikely to hit a peak.

For our purpose, convolution, what really needs to hold, is that $\hat{f}^n * h_n^{-n} = f * h_n$, for any piecewise polynomial kernel h_n of degree $n - 1$. This includes also very compact h_n , so as to prevent the antiderivative network to “cheat” by not learning the antiderivative of the signal but the antiderivative of a convolution of the signal.

The resulting loss to achieve this is

$$\mathbb{E}_{\mathbf{x} \in d_{in}} \left\| \left\| \sum_{i=1}^m \hat{f}^n(\mathbf{x} - \mathbf{x}^{(i)}) w^{(i)} - \mathbb{E}_{\mathbf{x}^{(1)} \leq \tau < \mathbf{x}^{(m)}} [f(\mathbf{x} - \boldsymbol{\tau}) h_n(\boldsymbol{\tau})] \right\| \right\|, \quad (11)$$

where $\mathbf{x}^{(i)}$ and $w^{(i)}$ are the Dirac delta positions and magnitudes of h_n^{-n} . The first term is due to Eq. 6 and the second term is a Monte Carlo estimate of the convolved signal.

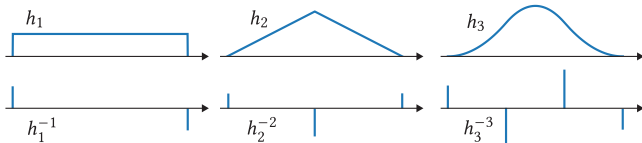


Fig. 8. Minimal piecewise polynomial kernels of different degrees (top row) and their corresponding Dirac deltas (bottom row).

We choose the n -th “minimal” kernel h_n to be the n -fold convolution of a box with itself (Fig. 8). Minimality has three main benefits: i) It is sufficient to force the network to learn the antiderivative; ii) the left part of the loss Eq. 11 becomes a sum over only $m = (n + 1)^d$ elements that is efficient to compute, corresponding to higher-order finite differences, and iii) the right part becomes the expectation over a tame interval around \mathbf{x} (the blue interval in Fig. 7), which greatly reduces variance and allows learning a high-quality integral field.

Table 2. Settings for all applications.

Modality	Input			Kernel				
	d_{in}	d_{out}	Format	Shape	SV	d	Order	m
Images	2	3	Grid	Gauss	×	2	Linear	169
	2	3	Grid	DoG	×	1	Linear	13
	2	3	Grid	Circle	✓	2	Const.	141
Video	3	3	Grid	Gauss	×	1	Linear	13
Geometry	3	1	SDF	Box	×	3	Const.	8
Animation	1	69	Paths	Gauss	×	1	Linear	13

4.4 Implementation Details

We have implemented our prototype within the PyTorch [Paszke et al. 2017] environment. All source code will be released upon publication. Our integral fields are realized using MLPs, where exact architectures vary depending on the modality to be represented. Similar to Lindell et al. [2021], we observed best quality with Swish [Ramachandran et al. 2017] activation functions.

For training our repeated integral field, we again use the Adam [Kingma and Ba 2014] optimizer with standard parameters. Considering a unit domain, we train with a size of 0.025 for the minimal kernel h_n until convergence, followed by a fine-tuning on a kernel of size 0.0125. To obtain stable solutions, we cannot decrease this size arbitrarily. Therefore our repeated integral field \hat{f}^n is a slightly low-pass filtered version of f^n , resulting in a lower limit of filter sizes our convolutions can faithfully compute. Fortunately, these small filters are highly amenable to efficient Monte Carlo estimation. Thus, at test time, whenever a kernel size falls below the threshold, we Monte-Carlo-estimate the convolution.

5 APPLICATIONS

To demonstrate the generality and efficiency of our approach, we consider four signal modalities: images, videos, geometry, and character animations. An overview of settings for all modalities is given in Tab. 2.

5.1 Images

In this application, we consider (high-dynamic range) RGB images as signals. We show result for Gaussian image filter in Fig. 9 and a derivative-of-Gaussians filter in Fig. 10.

In Table 3 and Fig. 11, we compare image quality of our approach using a piecewise linear kernel to the state-of-the-art method INSP [Xu et al. 2022] for differently-sized Gaussians. Similar to our approach, INSP relies on higher-order derivatives, but uses them in a point-wise fashion to reason about local neighborhoods, reminiscent of a Taylor expansion. We follow their original implementation and provide all second-order partial derivatives. We found that providing more derivatives did not markedly improve their results. We evaluate image quality on a set of 50 images. We observe that our approach outperforms INSP on all kernels, with the difference between the methods getting more significant as the kernel size increases.

Further, we demonstrate spatially-varying convolutions in Fig. 1 and Fig. 13. In these cases, the strength of a circular blur filter is

Table 3. Image quality comparison for Gaussian kernels.

	$\sigma = 0.04$			$\sigma = 0.05$			$\sigma = 0.07$		
	PSNR	LPIPS	SSIM	PSNR	LPIPS	SSIM	PSNR	LPIPS	SSIM
INSP	27.14	0.34	0.77	25.48	0.44	0.71	23.64	0.57	0.61
Ours	26.45	0.10	0.88	27.76	0.06	0.90	28.04	0.06	0.91

determined by a spatially-varying auxiliary signal in the form of a depth buffer.



Fig. 9. Gaussian 2D image blur of the input signal, with increasing bandwidth. It can be seen how our approach works also for large kernels. References look visually indistinguishable, as seen from the supplemental.

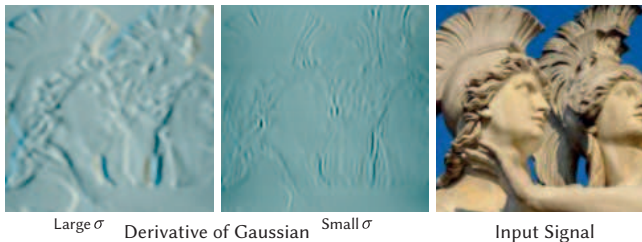


Fig. 10. Derivative-of-Gaussian filtering 2D result. Note, that our approach supports such non-convex filters, producing signed results.

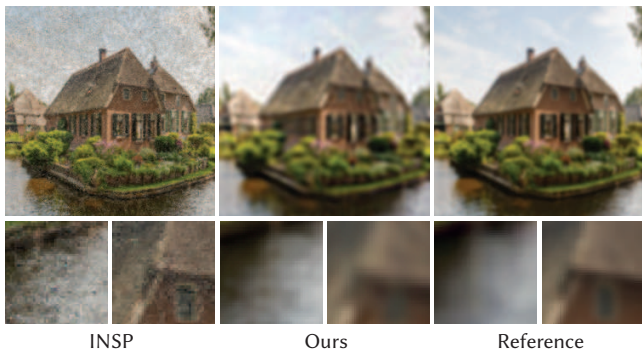


Fig. 11. A qualitative comparison between INSP [Xu et al. 2022] and our approach using a Gaussian kernel. Their approach does hardly perform any filtering, when the kernel is larger, such as our approach supports, but suffers from noise.

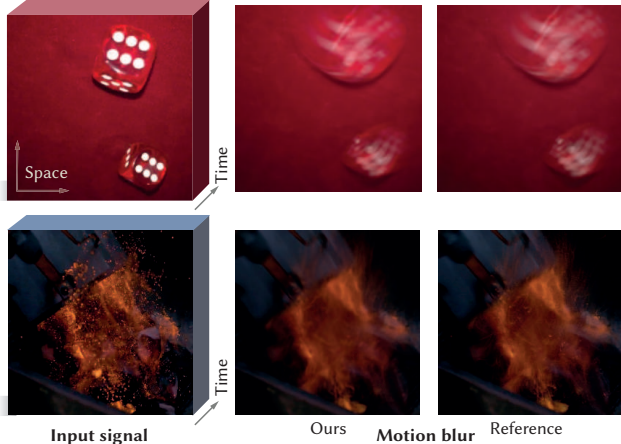


Fig. 12. We apply our approach to a 3D space-time HDR field (video, seen left) to filter along the time axis with a Gaussian kernel. The resulting motion blur (middle) compares favorably to a reference computed using MC.

5.2 Videos

Videos are fields $f \in \mathbb{R}^3 \rightarrow \mathbb{R}^3$, mapping 2D location and time to RGB color. In Fig. 12, we apply Gaussian smoothing along the time dimension to create appealing non-linear motion blur. We refer to our supplemental material for a more extensive evaluation.



Fig. 13. Depth-of-field applied to a synthetic image with a depth map.

5.3 Geometry

Surfaces can be modeled using signed distance functions (SDFs) $f \in \mathbb{R}^3 \rightarrow \mathbb{R}$. In Fig. 14, we apply differently sized 3D box filters to an SDF, resulting in a progressively smoothed surface.



Fig. 14. A geometric shape represented by an SDF is filtered with a box kernel of two different sizes. Low-pass filtering of an SDF naturally results in morphological simplifications. With our approach, this neural field convolution requires only eight network evaluations, independent of kernel size.

5.4 Animation

Finally, we consider the task of filtering a neural field representation of a motion-capture sequence, which contains a significant amount of noise. Our test sequence consists of 23 3D joint position paths over time, resulting in a field $f \in \mathbb{R} \rightarrow \mathbb{R}^{69}$. In Fig. 15, we show the result of applying a Gaussian filter to the noisy animation data, resulting in smooth motion trajectories.

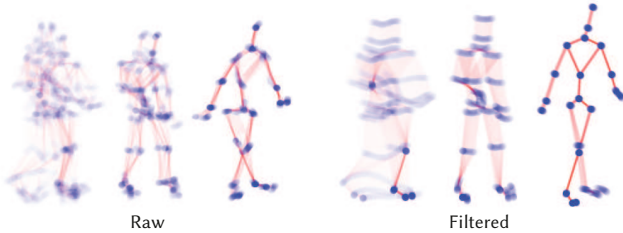


Fig. 15. A noisy motion-capture sequence (left) is filtered using our approach to yield smooth motion trajectories (right).

6 CONCLUSION

We have presented a novel approach to perform general, spatially-varying convolutions in continuous signals. Capitalizing on the fact that piecewise polynomial kernels become sparse after repeated differentiation, we only require a small number of integral-network evaluations to perform large-scale continuous convolutions.

Since our work is one of the first steps in this direction, there is ample opportunity for future work. Currently, one of our biggest limitations is that we need access to the entire signal to train our repeated integral field. This prevents the treatment of signals that are only partially observed through a differentiable forward map, e.g., as prominently is the case for neural radiance fields [Mildenhall et al. 2020]. Further, kernel transformations are limited to axis-aligned operations. We envision that re-parameterizations leveraging the continuous nature of the representation might be able to lift this restriction.

We hope to inspire future work on signal processing in continuous neural representations to help them reach their full potential.

REFERENCES

Jonathan T. Barron, Ben Mildenhall, Matthew Tancik, Peter Hedman, Ricardo Martin-Brualla, and Pratul P. Srinivasan. 2021. Mip-NeRF: A Multiscale Representation for Anti-Aliasing Neural Radiance Fields. *ICCV* (2021).

Jonathan T. Barron, Ben Mildenhall, Dor Verbin, Pratul P. Srinivasan, and Peter Hedman. 2022. Mip-NeRF 360: Unbounded Anti-Aliased Neural Radiance Fields. *CVPR* (2022).

E Oran Brigham. 1988. *The fast Fourier transform and its applications*. Prentice-Hall, Inc.

Franklin C Crow. 1984. Summed-area tables for texture mapping. In *SIGGRAPH*. 207–212.

Yilun Du, M. Katherine Collins, B. Joshua Tenenbaum, and Vincent Sitzmann. 2021. Learning Signal-Agnostic Manifolds of Neural Fields. In *NeurIPS*.

Emilien Dupont, Hyunjik Kim, SM Eslami, Danilo Rezende, and Dan Rosenbaum. 2022. From data to functa: Your data point is a function and you should treat it like one. *arXiv preprint arXiv:2201.12204* (2022).

Emilien Dupont, Yee Whye Teh, and Arnaud Doucet. 2021. Generative models as distributions of functions. *arXiv preprint arXiv:2102.04776* (2021).

Zeev Farbman, Raanan Fattal, and Dani Lischinski. 2011. Convolution pyramids. *ACM Trans. Graph.* 30, 6 (2011), 175.

Paul S Heckbert. 1986. Filtering by repeated integration. *ACM SIGGRAPH Computer Graphics* 20, 4 (1986), 315–321.

Pedro Hermosilla, Tobias Ritschel, Pere-Pau Vázquez, Àlvar Vinacua, and Timo Ropinski. 2018. Monte carlo convolution for learning on non-uniformly sampled point clouds. *ACM Trans. Graph.* 37, 6 (2018), 1–12.

Amir Hertz, Or Perel, Raja Giryes, Olga Sorkine-Hornung, and Daniel Cohen-Or. 2021. Sape: Spatially-adaptive progressive encoding for neural optimization. *NeurIPS* 34 (2021), 8820–8832.

Brian KS Isaac-Medina, Chris G Willcocks, and Toby P Breckon. 2022. Exact-NeRF: An Exploration of a Precise Volumetric Parameterization for Neural Radiance Fields. *arXiv preprint arXiv:2211.12285* (2022).

Diederik P Kingma and Jimmy Ba. 2014. Adam: A method for stochastic optimization. *arXiv preprint arXiv:1412.6980* (2014).

Georgios Kopanas, Thomas Leimkühler, Gilles Rainer, Clément Jambon, and George Drettakis. 2022. Neural Point Catacaustics for Novel-View Synthesis of Reflections. *ACM Trans. Graph.* 41, 6 (2022), Article–201.

Thomas Leimkühler, Hans-Peter Seidel, and Tobias Ritschel. 2018. Laplacian Kernel Splatting for Efficient Depth-of-field and Motion Blur Synthesis or Reconstruction. *ACM Trans. Graph. (Proc. SIGGRAPH)* 37, 4 (2018), <https://doi.org/10.1145/3197517.3201379>

Tony Lindeberg. 2013. *Scale-space theory in computer vision*. Vol. 256. Springer Science & Business Media.

David B Lindell, Julien NP Martel, and Gordon Wetzstein. 2021. Autoint: Automatic integration for fast neural volume rendering. In *CVPR*. 14556–14565.

Ben Mildenhall, Pratul P Srinivasan, Matthew Tancik, Jonathan T Barron, Ravi Ramamoorthi, and Ren Ng. 2020. Nerf: Representing scenes as neural radiance fields for view synthesis. In *ECCV*. 405–421.

Thomas Müller, Alex Evans, Christoph Schied, and Alexander Keller. 2022. Instant Neural Graphics Primitives with a Multiresolution Hash Encoding. *ACM Trans. Graph.* 41, 4, Article 102 (2022), 102:1–102:15 pages.

Jeong Joon Park, Peter Florence, Julian Straub, Richard Newcombe, and Steven Lovegrove. 2019. DeepSDF: Learning continuous signed distance functions for shape representation. In *CVPR*. 165–174.

Keunhong Park, Utkarsh Sinha, Jonathan T Barron, Sofien Bouaziz, Dan B Goldman, Steven M Seitz, and Ricardo Martin-Brualla. 2021. Nerfies: Deformable neural radiance fields. In *ICCV*. 5865–5874.

Adam Paszke, Sam Gross, Soumith Chintala, Gregory Chanan, Edward Yang, Zachary DeVito, Zeming Lin, Alban Desmaison, Luca Antiga, and Adam Lerer. 2017. Automatic differentiation in pytorch. (2017).

Prarit Ramchandran, Barret Zoph, and Quoc V Le. 2017. Searching for activation functions. *arXiv preprint arXiv:1710.05941* (2017).

Nicholas Sharp and Alec Jacobson. 2022. Spelunking the Deep: Guaranteed Queries on General Neural Implicit Surfaces via Range Analysis. *ACM Trans. Graph.* 41, 4, Article 107 (2022).

Assaf Shocher, Ben Feinstein, Niv Haim, and Michal Irani. 2020. From discrete to continuous convolution layers. *arXiv preprint arXiv:2006.11120* (2020).

Patrice Simard, Léon Bottou, Patrick Haffner, and Yann LeCun. 1998. Boxlets: a fast convolution algorithm for signal processing and neural networks. *NeurIPS* 11 (1998).

Vincent Sitzmann, Julien Martel, Alexander Bergman, David Lindell, and Gordon Wetzstein. 2020. Implicit neural representations with periodic activation functions. *NeurIPS* 33 (2020), 7462–7473.

Vincent Sitzmann, Michael Zollhöfer, and Gordon Wetzstein. 2019. Scene Representation Networks: Continuous 3D-Structure-Aware Neural Scene Representations. In *NeurIPS*.

Kenneth O Stanley. 2007. Compositional pattern producing networks: A novel abstraction of development. *Genetic programming and evolvable machines* 8 (2007), 131–162.

Matthew Tancik, Pratul Srinivasan, Ben Mildenhall, Sara Fridovich-Keil, Nithin Raghavan, Utkarsh Singhal, Ravi Ramamoorthi, Jonathan Barron, and Ren Ng. 2020. Fourier features let networks learn high frequency functions in low dimensional domains. *NeurIPS* 33 (2020), 7537–7547.

Ayush Tewari, Justus Thies, Ben Mildenhall, Pratul Srinivasan, Edgar Tretschk, W Yifan, Christoph Lassner, Vincent Sitzmann, Ricardo Martin-Brualla, Stephen Lombardi, et al. 2022. Advances in neural rendering. *Comp. Graph. Forum* 41, 2 (2022), 703–735.

Edgar Tretschk, Ayush Tewari, Vladislav Golyanik, Michael Zollhöfer, Christoph Lassner, and Christian Theobalt. 2021. Non-rigid neural radiance fields: Reconstruction and novel view synthesis of a dynamic scene from monocular video. In *ICCV*. 12959–12970.

Cristina Vasconcelos, Kevin Swersky, Mark Matthews, Milad Hashemi, Cengiz Oztireli, and Andrea Tagliasacchi. 2022. CUF: Continuous Upsampling Filters. *arXiv preprint arXiv:2210.06965* (2022).

Delio Vicini, Sébastien Speierer, and Wenzel Jakob. 2022. Differentiable signed distance function rendering. *ACM Trans. Graph.* 41, 4 (2022), 1–18.

Paul Viola and Michael Jones. 2001. Rapid object detection using a boosted cascade of simple features. In *CVPR*, Vol. 1. I–I.

- Shenlong Wang, Simon Suo, Wei-Chiu Ma, Andrei Pokrovsky, and Raquel Urtasun. 2018. Deep parametric continuous convolutional neural networks. In *CVPR*. 2589–2597.
- Yinhui Wang, Shuzhou Yang, Yujie Hu, and Jian Zhang. 2022. NeRFocus: Neural Radiance Field for 3D Synthetic Defocus. *arXiv preprint arXiv:2203.05189* (2022).
- Lance Williams. 1983. Pyramidal parametratics. In *SIGGRAPH*, Vol. 17. 1–11.
- Andrew P Witkin. 1987. Scale-space filtering. In *Readings in Computer Vision*. 329–332.
- Yiheng Xie, Towaki Takikawa, Shunsuke Saito, Or Litany, Shiqin Yan, Numair Khan, Federico Tombari, James Tompkin, Vincent Sitzmann, and Srinath Sridhar. 2022. Neural fields in visual computing and beyond. *Comp. Graph. Forum* 41, 2 (2022), 641–676.
- Dejia Xu, Peihao Wang, Yifan Jiang, Zhiwen Fan, and Zhangyang Wang. 2022. Signal Processing for Implicit Neural Representations. In *NeurIPS*.
- Guandao Yang, Serge Belongie, Bharath Hariharan, and Vladlen Koltun. 2021. Geometry processing with neural fields. *NeurIPS* 34 (2021), 22483–22497.
- Yu-Jie Yuan, Yang-Tian Sun, Yu-Kun Lai, Yuewen Ma, Rongfei Jia, and Lin Gao. 2022. NeRF-editing: geometry editing of neural radiance fields. In *ICCV*. 18353–18364.
- Xian-Da Zhang. 2022. Modern signal processing. In *Modern Signal Processing*. De Gruyter.